Accepted manuscript doi:
10.1680/jgeot.24.01059

Submitted: 03 April 2024

Published online in 'accepted manuscript' format: 10 December 2024

Manuscript title: Investigating alternative foundation systems for offshore wind turbines in liquefiable soils

Authors: C. Español-Espinel[*], D. Gaudio[*,†] and S. P. G. Madabhushi[*]

Affiliations: [*]Department of Engineering, University of Cambridge, CB3 0EF, Cambridge, UK, [†]Department of Structural and Geotechnical Engineering, Sapienza University of Rome, Via Eudossiana 18, 00184 Rome, Italy

Corresponding author: C. Español-Espinel, Department of Engineering, University of Cambridge, CB3 0EF, Cambridge, UK

E-mail: ce411@cam.ac.uk

Accepted manuscript doi:
10.1680/jgeot.24.01059

Abstract

As the offshore wind industry expands into southeast Asia and west coast of USA, the seismic considerations become important in the design of the foundations, especially when liquefaction of shallow layers can occur under seismic loading. This paper presents centrifuge modelling of three foundation systems for offshore wind turbines installed in liquefiable soil, specifically a monopile, a composite system with a monopile and an outrigger, and an outrigger only system. The study discusses the performance of the three foundations in supporting identical offshore wind turbines subjected to a combination of operational and earthquake loading. The rotational stiffness of these three foundations is investigated before, during and after the seismic loading. The key findings suggest that the monopile experiences earthquake-induced rotation exceeding the allowable threshold recommended by DNV-ST-0126 (2021) and DNV-RP-0585 (2021). Although the hybrid foundation is expected to perform better compared to the monopile and the outrigger as separate foundations, the outrigger as a standalone structure is the foundation that exhibits less rotation. However, this advantage comes at the cost of larger settlements. Overall, the outrigger only foundation provided a reasonably consistent solution for supporting offshore wind turbines in areas prone to liquefaction induced by earthquakes.

Keywords: offshore renewable energy, liquefaction, centrifuge modelling, foundation engineering, seismic engineering

Accepted manuscript doi:
10.1680/jgeot.24.01059

Introduction

Offshore wind technology had its early implementation in Europe, notably in the North Sea and Baltic Sea, where the monopile emerged as the preferred foundation system for Offshore Wind Turbines in shallow waters. Monopiles have proven to be a successful solution to support Offshore Wind Turbines (OWTs) in terms of design, ease of installation, and large-scale production.

Other regions in the world, including Japan and Taiwan, where there is a growing interest in deploying offshore wind energy, base their OWTs and foundation systems on European experiences. In these areas, earthquakes pose challenges for current foundation systems such as monopiles and jackets, which were not originally designed to withstand seismic loading and liquefaction (Fig. 1).

Early research on the effects of earthquakes on offshore wind turbines focused on assessing whether the structural capacity of the turbines could be exceeded when subjected to combined operational and seismic loading (Asareh et al., 2016, Smith and Mahmoud, 2016).

Earthquake loading is more likely to compromise the serviceability limit state (SLS) of the turbines rather than their structural capacity. This is due to earthquake-induced rotation and settlement, which could become driving factors in the design. Based on this, Kaynia (2018) suggests adopting performance-based approaches for the seismic design of offshore wind turbines. While this methodology produces more cost-effective designs, it often depends on project-specific criteria which are not standardised across the industry.

Accepted manuscript doi:
10.1680/jgeot.24.01059

For this reason, several companies and institutions, including ARUP, Ørsted, Shell, Shimizu, Mitsubishi, Siemens Gamesa, Vestas, and many others have launched ACE and ACE 2 (Alleviating Cyclone and Earthquake Challenges), two joint industry projects (JIP) organised by the certifier DNV to make the design process for Offshore Wind Turbines subjected to seismic loading more reliable. The first edition of this initiative resulted in the recommended practice for seismic design for wind power plants DNV-RP-0585 (2021), whereas ACE 2 aims at updating this standard by addressing specific topics such as damping and liquefaction. The guideline prescribes that foundation designs for OWTs in earthquake prone regions should be verified against the combined action of seismic and operational loading as one of the most important design load cases.

This scenario becomes critical when considering monopile supported OWTs installed in soils susceptible to liquefaction, which would alter the horizontal effective stress exerted by the soil on the monopile. In other words, the soil may not be capable of reacting against the loads transferred by the foundation leading to significant rotation of the OWT. This problem has been previously studied by Esfeh & Kaynia (2020), who conducted Finite Difference analyses on 6 m diameter monopiles in liquefiable soil exposed to earthquake loading combined with static or cyclic loading from wind and waves. Espanol-Espinel et al. (2023) also carried out simplified finite element analyses to investigate liquefaction within the soil plug enclosed inside the monopile. They concluded that for large diameter monopiles, the soil plug may be vulnerable to liquefaction caused by seismic loading.

Accepted manuscript doi:
10.1680/jgeot.24.01059

In addition, Espanol-Espinel *et al*. (2024) conducted centrifuge modelling of 7.11 m monopiles subjected to a combination of dynamic loading that induced liquefaction within the soil, and static lateral loading. Both studies revealed significant rotation of the monopile and superstructure that exceeded by far, the allowable threshold of 0.5° set by DNV-ST-0126 (2021) and DNV-RP-0585 (2021). On the other hand, the centrifuge experiments carried by Natarajan and Madabhushi (2022) on jacket structures supported by pin piles suggested less rotation compared to that predicted for monopiles, but still larger than acceptable limits suggested by DNV-ST-0126 (2021). This is ascribed the separation distance between the pin piles under each of the jacket legs, which grants jacket structures additional moment resistance. Based on this observation, the present paper proposes a novel foundation system described as an outrigger consisting of four legs with skirted footings at their ends. The substructure has been modelled using the Turner Beam Centrifuge at the University of Cambridge. The outrigger has initially been designed to complement the monopile, giving rise to a hybrid foundation system. Previous research on composite foundations that amalgamated monopiles, circular footings and caissons revealed the potential benefits provided by these structural modifications to the overall performance of the structure. Shakeran and Soroush (2024), conducted centrifuge modelling of hybrid suction caissons consisting of shallow foundations with an internal caisson. The foundations were installed in saturated medium-dense sand and subjected to 600 cycles of long-term cyclic loading.

Anastasopoulos and Theofilou (2016), compared the response of a 30 m long monopile embedded in clay, subjected to operational and seismic loading, with that of a hybrid foundation

combining a 15 m long monopile with a circular footing. Both the foundation and superstructure were modelled using 3D FE, and the key findings suggest that a footing with at least a 20 m diameter was required to surpass the performance of the 30 m long monopile. More relevant to this research, Chen et al., (2023) undertook 3D FE modelling of a 5MW offshore wind turbine exposed solely to seismic loading and supported by a hybrid foundation in liquefiable soil. The foundation included a 45 m long monopile paired with a 10 m diameter wide-shallow bucket. The resistance to liquefaction around the monopile improved due to the reduced accumulation of excess pore pressure beneath the bucket.

In the present research, the outrigger is tested as both a standalone solution and in conjunction with a monopile. The performance of these configurations is compared to that of a monopile under combined earthquake and operational loading.

TEST DESIGN AND METHODOLOGY

This research aims at comparing the response of three different foundation systems for OWTs against combined static lateral loading and earthquake loading using centrifuge testing. In the first experiment, a monopile foundation was tested (Fig. 2). The results of the initial experiment led to the development of structural modifications to the monopile to overcome the detrimental effects of earthquake-induced liquefaction, inertial loading, and operational loading on the OWT. The structure tested in the second experiment was a monopile combined with a four-legged cruciform foundation with a skirted footing at the end of each leg, referred to as an outrigger (Fig. 3a), while the third test was intended to understand the performance of the outrigger on its own (Fig. 3b). All tests were run at a centrifuge acceleration of 70g.

Experimental setup

The soil profile selected for testing of the three foundation systems included a 7-m-thick loose sand layer with $D_R \approx 40\%$, overlying a 15.4 m dense sand layer with $D_R \approx 90\%$. The sand sample was pluviated inside the ESB (Equivalent Shear Beam) model container using the automatic sand pourer at the University of Cambridge (Madabhushi et al., 2006). The ESB box (Brennan et al., 2006) is designed as a deck of rectangular aluminium frames interbedded with rubber sheets which increase in thickness towards the top of the container. Gaudio *et al*. (2023) suggested that the boundary effects of the ESB box in dynamic centrifuge testing result in less than a 20% deviation of the measured model response compared to free-field boundary conditions. To minimize spurious boundary effects, the foundations were installed at distances of 5.5 times the diameter for the monopile and 3.2 times the diameter for the caissons from the ESB box boundary perpendicular to the direction of shaking. Other popular solutions to restrict size effects in dynamic centrifuge modelling are laminar containers. Unfortunately, the size of the existing laminar box at the University of Cambridge is insufficient to accommodate the models proposed in this paper.

Sand pouring was followed by full saturation of the loose and dense sand layers using the Cam-Sat System (Stringer and Madabhushi, 2009). This is a two-phase procedure in which the pores of the sand sample are filled with CO_2 to be subsequently saturated with a high-viscosity methylcellulose solution. CO_2 is more soluble than air in the viscous fluid, which improves saturation of the soil sample. The viscosity of the saturation fluid is augmented by a factor of 70, which is the scaling factor of the experiment, to satisfy the scaling laws for velocity and time in

dynamic events (Madabhushi, 2014). This ensures that during the co-seismic phase, the excess pore pressure accumulates at the same rate at which it dissipates during the post-seismic phase.

After completing the preparation of the soil sample, each of the foundation systems considered in this series of experiments was installed at 1g. In the case of the monopile, a hydraulic press was used to drive the foundation to the scheduled depth. Following this, the OWT tower was assembled above each of the foundations.

High-gravity installation may induce additional horizontal stresses within monopiles as suggested by Espanol-Espinel *et al*. (2023), and around them. Although Stringer and Madabhushi (2011) indicated that the axial behaviour is not adversely affected by 1*g* installation, the influence on the lateral response may be more significant. In-flight installation requires additional actuators to drive the monopile, which poses a challenge for the subsequent assembly of the tower.

The operational moment at the mudline due to wind thrust and waves was reproduced using a loading rig (Fig. 2). This device was specifically designed to apply lateral load to the RNA of the turbine. The structure of the loading rig consists of a base plate that rests on the edges of the ESB box, and a U channel vertically mounted on its right end. The topmost section of the U channel supports a pulley and is linked to the base plate using two struts that work in compression and tension to restrict the vibrations of the channel during dynamic loading. The static lateral load is applied using hanging mass which is connected to the RNA by means of a steel wire that rests on the pulley. During the swing up process, the hanging mass is supported by a piston placed inside the U channel. Once the desired centrifuge acceleration is reached, the piston is retracted to

release the hanging mass and apply the lateral load. The hanging mass provides a static lateral load of 0.367 MN, which generates a moment of 20 MNm at ground level (Table 1).

Properties of the Foundations

As shown in Fig. 2, the diameter and length of the monopile tested was 4 m and 17.5 m respectively, whereas the height of the Rotor-Nacelle Assembly (RNA) from ground level was 53.30 m. Despite these dimensions being 2.25 times smaller than those of full-scale structures in the field, the aspect (L/D) and the eccentricity (e/D) ratios are comparable to those of real structure values (Tab. 1). Therefore, to replicate the behaviour that real monopile supported offshore wind turbines would exhibit against static lateral loading, the static moment at ground level was also scaled down by a factor of 2.25. Distance scales times the scaling factor, whereas moment scales with the scaling factor to the cube as per the centrifuge scaling laws (Madabhushi, 2014).

The outrigger is a cruciform-shaped structure with four 9.1 m long legs that extend from the base of the OWT at an angle of 15° on either side of the shaking axis, meaning that they are almost parallel to the direction of shaking (Fig. 4). The ends of the legs rest on 3.15 m diameter skirted footings that are driven to a depth of 3.5 m into the loose sand (Tab. 2). In reality, the outrigger foundation is intended to be built with their legs perpendicular to each other. However, this setup was not feasible given the reduced width of the ESB model container. The experiment may be repeated using a model container with larger dimensions to allow for a more realistic deployment of the legs.

The Factor of Safety for vertical load of the monopile and outrigger are comparable as summarised in Tab.3. Moreover, the composite foundation combines the vertical capacities of the two previous foundations, resulting in a significantly larger Factor of Safety.

Loading Sequence

Each of the turbines supported by the foundations presented in this paper, the monopile, the monopile and outrigger, and the outrigger, were subjected to the loading sequence summarised in Tab. 4. For brevity, only the results obtained from the static loading, unloading and reloading phases, and earthquakes EQ1 and EQ2 are discussed in the current study. The static lateral loading is exerted through the piston-based mechanism described in Section *Experimental setup*, while the earthquake motions are reproduced by means of a servo-hydraulic earthquake actuator that seats on one end of the beam centrifuge. The OWT model is then loaded on top of the earthquake actuator, which is operated by means of a highly pressurised oil system and a servo-valve that controls the oil flow rate. At the time of the earthquake, the required displacement time-history is transferred to the servo-valve which translates the oil flow into motion (Madabhushi *et al*., 2015).

EQ1 consists of a sine sweep which shakes the OWT tower with a broad spectrum of frequencies at a very low Peak Ground Acceleration (PGA). This motion facilitates identifying the excitation frequencies of the superstructure. Following this, the tower is loaded laterally so that the OWT is subjected to combined static and dynamic loading during the second earthquake (EQ2). Before advancing to EQ3, the static lateral load is unloaded and subsequently reapplied before EQ4. EQ2, EQ3 and EQ4 are 1Hz frequency signals which last for 10 cycles. The aim of these input

accelerations is to generate enough excess pore water pressure within the soil to trigger liquefaction. The main advantage of using single known frequency signals for EQ2, EQ3 and EQ4 is that the effects of earthquakes cycles on the soil and the dynamic response of the OWT are easily identifiable. Signals with multiple frequencies may cause excitation of specific modes of the superstructure, which may lead to a more complex response of the foundation and OWT tower.

Instrumentation

Assessing the soil behaviour under dynamic loading in different regions of the model is one of the key priorities in the experiments presented in this paper. Thus, Pore Pressure Transducers (PPTs) and piezoelectric accelerometers were vertically distributed across the far-field of the model to record excess pore water pressure and ground acceleration respectively. In addition, PPTs were also placed below the skirted footings of the outrigger (Fig. 3) and on the leeward side of the monopile (Fig. 2 and 3). The settlements on the windward and leeward sides of the OWT were measured using Linear Variable Differential Transformers (LVDTs). This data together with the acceleration recorded by Micro Electro-Mechanical Systems (MEMS) located at the base of the tower were used to assess and cross check the amount of rotation experienced by the OWT. MEMs were also attached to the tower and the RNA mass to collect data on the dynamic response of the superstructure. The static lateral loading and the dynamic loading generated by the hanging mass and the RNA mass respectively, were recorded by a load cell that links one end of the wire that holds the hanging mass with the RNA. Most of the physical magnitudes recorded by the sensors, are driven by the input motion. Hence, although the base

displacement was an input of the shaker, the base acceleration was duly recorded by two piezo accelerometers. All data were recorded at a sampling frequency of 6000 Hz and filtered using an 8th order Butterworth low-pass filter with a cut-off frequency of 500 Hz.

STATIC LOADING

Fig. 5 illustrates the moment-rotation response recorded for the three foundation systems during the static Loading, Unloading and Reloading phases summarised in Table 4. It is apparent that the curves progress in steps. This is due to the mechanism through which the structure is laterally loaded and unloaded. Fig. 2 illustrates the piston that supports the hanging mass using pressurised air, which is regulated using a manually activated dial located in the centrifuge control room. The load cell at the RNA records the increase or decrease in lateral load as the pressure is gradually increased or decreased, giving rise to a step-shaped moment-rotation response.

From Fig. 5 it is evident that, for a given foundation system (*i.e.*, for a given plot in the Figure), the secant slope of the moment-rotation curve did not change remarkably across the Loading Unloading and the Reloading phases, except for the case of the outrigger as a standalone structure, where the Reloading curve is steeper than the other two. This result can be quantified referring to the secant rotational stiffness of the foundation system, $K_{\square\square}$, here defined using the following simplified form:

$$K_{\theta\theta} = \frac{\Delta M}{\Delta \theta} \tag{1}$$

where $\square M$ and $\square\square$ are the range of moment and rotation spanned by the foundation system, respectively. The simplifying assumption in the above definition relates to the coupled behaviour

Accepted manuscript doi:
10.1680/jgeot.24.01059

of the embedded foundations considered in this study (Shadlou and Bhattacharya, 2016), which was neglected in Eq. (1). The hypothesis is justified by the noticeable height of the superstructure, which therefore implied a high value for the eccentricity ratio, e/D (see Tab. 1): hence, the foundation behaviour can be expected to be mainly governed by pure rocking rather than by coupled swaying-rocking behaviour.

The secant rotational stiffnesses $K_{\square\square}$ values obtained are listed in Tab.5 for all the systems considered in the study. The rotational stiffness of the Outrigger as a standalone structure is the largest among the three foundations discussed (Tab.5), roughly double than that of the monopile.

As for the monopile and outrigger composite foundation (second line in Tab. 5), the values of $K_{\square\square}$ are between those of the two previous cases, which may be perceived as a counterintuitive result at a first glance. One possible explanation for this is that the bearing pressures generated underneath the skirted footings are smaller in the composite foundation, compared to the outrigger only case. When a lateral load is applied at the RNA level, the resulting moment is carried less well by the skirted footings in the composite foundation, resulting in a lower rotational stiffness compared to the outrigger as an independent structure.

In addition, the monopile and the outrigger as standalone foundations exhibit increments in rotational stiffness $K_{\square\square\square\square}$across the Loading, Unloading and Reloading phases (Tab. 5). These variations may be related to the effects of soil liquefaction triggered by EQ2 and EQ3, which occur after the Loading and Unloading stages respectively. Two concurring mechanisms may be resorted to explain this outcome. First, effective stresses in the soil were recovered after the occurrence of liquefaction, which would bring the rotational stiffness towards the pre-earthquake

values; then, second order effects may have contributed to this stiffness enhancement with respect to the pre-earthquake conditions, such as soil densification and the foundation embedment caused by the permanent settlement of the OWT. Clearly, the triggering of soil liquefaction involved some dynamic, permanent tilting, and settlement for the OWT, as discussed in the next section.

EARTHQUAKE LOADING

This section addresses the dynamic response of the offshore wind turbine and the hanging mass used to apply the lateral load. Furthermore, the performance of the monopile, the monopile and outrigger composite foundation, and the outrigger in liquefiable soils is explored.

Dynamic Response of the Superstructure

The dynamics of the OWT superstructure are of fundamental interest in this research. Thus, the lumped mass representing the RNA (Fig. 2) and the bending stiffness of the OWT tower were adjusted to achieve a natural frequency (f_n) similar to that of a DTU 10 MW reference offshore wind turbine. Shaofeng *et al*. (2021) suggested that the allowable natural frequency range between the 1P and 3P harmonics for the DTU 10 MW turbine is 0.16 Hz to 0.28 Hz. Alkhoury *et al*. (2020) predicted the first and second bending modes of excitation at 0.20 Hz and 1.44 Hz respectively. Fig 6 illustrates the frequencies at which the prototype offshore wind turbine experiences excitation upon the application of the sine sweep (EQ1) for the three foundation scenarios proposed. The first natural frequency of the prototype is encountered at 0.20 Hz, the value predicted by Alkhoury *et al*. (2020) for a DTU 10 MW turbine. However, no response is exhibited at the second mode of excitation.

During shaking, the loadcell reads the static lateral loading generated by the hanging mass in addition to the dynamic loading. The hanging mass and the RNA behave like two masses connected by a spring. Although the response of this system differs slightly from that of the tower and RNA mass, the contribution of the hanging mass to the dynamic loading is relatively minor. The authors acknowledge that this is an artifact of the system designed to apply the static lateral loading.

Fig. 7 depicts the influence of the hanging mass in the dynamics of the tower and RNA for the monopile case during earthquake EQ2. A comparison is made between:

- The moment at ground level obtained from the load cell when the tower is subjected to static lateral loading and dynamic loading combined (blue).
- The dynamic moment at ground level calculated using the mass and acceleration of the RNA in the laterally loaded scenario (red).
- The dynamic moment at ground level calculated using the mass and acceleration of the RNA in the non-laterally loaded scenario (green).

Under tension (positive), the dynamic moment recorded by the loadcell reaches similar values to that calculated using the acceleration at the RNA. Under compression (negative), the wire holding the hanging mass is not capable of transferring the load to the RNA and therefore, the dynamic moment is close to 0. The dynamic moment obtained from the acceleration at the RNA for both, the laterally loaded and non-laterally loaded cases is very similar. Hence, the influence of the hanging mass is considered not significant.

Performance of the Foundations against Soil Liquefaction

As summarised in Section *Loading Sequence*, earthquake EQ2 fired in this series of experiments is intended to liquefy the soil. The vertical array of sensors located in the far-field (Fig. 2, Fig. 3) detects enough accumulation of excess pore water pressure (u_{excess}) to exceed the vertical effective stress (σ'_{v0}) and trigger liquefaction (Fig. 8). The liquefaction threshold at the far-field is described as:

$$\sigma'_{v0} = \sigma_{v0} - u_{hyd} \quad (2)$$

where σ_{v0} is the geostatic total vertical stress and u_{hyd} is the hydrostatic pore pressure. Excess pore pressure does not increase following a constant trend but exhibits intermittent drops before reaching its peak (Fig.8). These occur due to dilation when the stress path of soil reaches the so-called Phase Transformation Line (Ishihara, 1993).

Soil liquefaction combined with the static lateral moment provided by the hanging mass, and the dynamic moment from the RNA mass itself, results in substantial rotation of the OWT (Fig.9). However, there are significant variations in the amount of rotation depending on the foundation system adopted. In the case of the monopile, most of the rotation takes place during earthquake EQ2, although the structure slightly rotates after the earthquake until reaching almost 2.85°. The addition of the outrigger to the monopile reduced the rotation of the structure from 2.85° to 0.65°. Earthquake induced rotation was further reduced to 0.3° when the outrigger was tested on its own. Following EQ2, the rotation increased progressively to 0.5°, which is the threshold allowed by DNV-ST-0126 (2021) and DNV-RP-0585 (2021).

The magnitude of the dynamic moment is larger than that of the static moment and may have a greater contribution to the overall rotation of the structure (Fig. 10). Nevertheless, the static

moment, which was applied in the same direction as the earthquake shaking, dictates the direction towards which the whole structure may tilt as discussed by Español-Espinel et al. (2024). As illustrated in Fig. 10, when the sum of the static and dynamic moments is at its maximum, very little rotation accumulates, while a lot more rotation accumulates when the static and dynamic moments are at their minimum. The load cell measures the tension exerted on the wire, which is the sum of the static load from the hanging mass and the dynamic load induced by the earthquake on the RNA mass. The maximum tension is recorded when the RNA moves towards the windward side, and the minimum tension occurs when the RNA moves towards the leeward side (Fig. 2). It is at this stage that the OWT undergoes further clockwise rotation.

In the case of the monopile foundation, the dynamic moment is greater compared to that acting on the outrigger alone (Fig. 11). This increase is probably due to the tip of the monopile being located at a greater depth, where the denser sand and higher effective stress prevent the sand from fully liquefying. As a result, shear waves are capable of propagating through the denser soil and the monopile. The outrigger, however, is embedded in a loose sand layer that fully liquefies during the earthquake, except beneath the skirted foundations. The liquefied layer tends to filter the shear stress generated by earthquake shaking, reducing the dynamic moment driving the rotation. In contrast, the monopile transfers the earthquake-induced shear stress to the superstructure more effectively.

Although the tip of the monopile is at the same depth in both, the monopile and the combined monopile and outrigger scenarios, the maximum dynamic moment is 26.2% smaller in the case of the composite foundation. In this scenario, the additional resistance provided by the outrigger

and skirted footings is probably reducing the amount of dynamic moment. This may have resulted in a smaller rotation, about four times smaller compared to the monopile.

In terms of rotation, the outrigger on its own performed better than the monopile and the composite foundation during and post-earthquake. Nevertheless, the OWT experienced higher settlement when supported by the outrigger (Fig. 12). In fact, the OWT and outrigger settled up to 365 mm during the earthquake, which is 28 % more than the monopile. The average earthquake induced settlement of the outrigger and monopile composite foundation was 130 mm, 54.4 % less than the monopile. In the 80 seconds following the earthquake, the OWT and outrigger foundation settled 97 additional mm, whilst the settlement of the composite foundation continued to increase by 10 mm. This represents 185 % more and 71 % less additional settlement compared to the monopile, for the outrigger and composite foundations, respectively.

Such differences in the performance of the three foundation systems may be attributed to the mechanisms through which each foundation transfers the self-weight of the superstructure, the operational loads i.e., wind and waves, and the inertial dynamic loading to the soil. The sign and magnitude of the excess pore pressure developed in the regions surrounding each foundation during and after the earthquake are indicative of the stress distribution in those areas. PPT-259 in the case of the monopile, and PPT-240 in the case of the hybrid foundation, recorded the excess pore pressure generated 1 monopile diameters far from the leeward side of the monopile (Fig. 13).

In the case of the monopile alone, PPT-259 recorded negative excess pore pressure with values of approximately -20 kPa, towards the 8^{th} cycle of EQ2. Thus, the monopile alone transfers stress

to the soil on the leeward side, which tends to dilate and generate suction. Conversely, PPT-240 recorded positive excess pore pressure of up to 25 kPa on the leeward side of the monopile of the composite foundation. Hence the stress transferred by the monopile part of the composite foundation is less significant and does not substantially contribute to resisting the static and dynamic moments.

Furthermore, the recordings of PPT-251 located 1.26 m below the skirted footing of the leeward side of the outrigger shows sharp oscillations of the excess pore pressure. These indicate strong dilation, meaning that liquefaction is not occurring in the soil immediately below the skirted footing. The monopile and outrigger foundation is therefore relying on the stress transferred by the skirted footings of the outrigger onto the soil to resist the static and dynamic moment. In light of these findings, it was hypothesised that the outrigger without the monopile could have a performance similar to that of the monopile and outrigger combined. In fact, the excess pore pressure recorded below the leeward skirted footing of the outrigger turned negative, whereas the pressures recorded beneath the leeward skirted footing of the hybrid foundation remained positive. (Fig. 14). In other words, the outrigger without monopile transfers higher amounts of stress to the soil below the skirted footings than the composite foundation. Additional evidence of suction within the soil below the outrigger foundation is provided in Fig. 15, showing negative excess pore pressure of -12 kPa (PPT-260) and -55 kPa (PPT-232) below the windward and leeward skirted footings, respectively.

Moreover, the excess pore pressure measured in the far-field, 4.2 m away from the leeward skirted footing, rises to positive values exceeding 40 kPa from the onset of the earthquake, while

the excess pore pressure below the skirted footings remains mostly negative. Eventually, the excess pore pressure reaches positive values similar to those recorded in the far-field due to pore fluid migration from areas where positive excess pore pressure developed during the earthquake.

DISCUSSION

Three different foundation systems for OWTs including a monopile, a monopile combined with an outrigger, and an outrigger on its own, were tested using dynamic centrifuge modelling at 70g. Each foundation withstood the self-weight of the OWT, the static moment generated by the lateral load applied at the RNA, and the dynamic moment due to the inertial loading of the tower and the RNA mass. The soil profile included a loose sand layer overlying a dense sand layer both of which were fully saturated. The earthquake motions were specifically selected to generate excess pore pressure and ultimately trigger full liquefaction of the sand layers.

Static loading

The foregoing outcomes from the static loading applied to the OWT demonstrate that the rotational stiffness of the foundation fully recovers after soil liquefaction occurs during a seismic event and in fact an increase in rotational stiffness was observed. This phenomenon is attributed to a combination of factors. First, the recovery of effective stresses after the dissipation of seismic-induced excess pore water pressures. Second, soil densification and further embedment of the foundation system caused by the settlement of the OWT.

Regarding the performance of the three foundation systems that were investigated, the initial expectation was that the composite foundation system, consisting of a monopile and an outrigger, would exhibit superior rotational stiffness. However, the results in Table 5 indicate

that the outrigger alone provides greater rotational stiffness. This is attributed to the differences in vertical stresses generated below the skirted footings in these two systems. For the outrigger only system, the vertical stress beneath the skirted footings is greater giving rise to a higher stiffness. For the composite system, the vertical stress below the skirted footings is lower as part of the vertical load is carried by the monopile. Thus, the soil stiffness beneath the skirted footings is lower, allowing for larger rotations when the moment due to the lateral load is applied to this system. This was an interesting and counter-intuitive result obtained in this research.

Earthquake loading

The findings of this research revealed significant differences in the performance of the three foundation types in terms of rotation (Fig. 9) and average settlement (Fig. 12). Rotation and average settlement immediately after the earthquake and 80 seconds after the end of the earthquake are summarised in Tab. 6 and Tab. 7 for each foundation system. As observed, the monopile rotated 2.50° during the earthquake and up to 2.85° within the 80 seconds that followed the earthquake, whereas the monopile and outrigger composite foundation reached 0.60° and 0.65° co-seismic and post-seismic respectively. Finally, the outrigger experienced 0.30° that increased to 0.50° in the same timescales. Thus, the outrigger foundation could reduce the rotation experienced by the OWT to values within the allowable range acknowledged by the technical guidelines (DNV-ST-0126, 2021 and DNV-RP-0585, 2021). While this advantage is accompanied by substantial settlements, these are generally considered to have a lesser impact on the seismic performance of offshore wind turbines compared to tilting.

The disparity in rotation and settlement experienced by the OWT in each case, and the rate of increase of these magnitudes after the earthquake depends on the mechanisms through which each foundation system transfers the loads affecting the superstructure onto the soil.

First, the monopile supports the self-weight of the superstructure above it by means of skin friction, meaning that shear stress is generated at the interface between the monopile and the surrounding sand. In addition, the static and dynamic moment resulting from operational and earthquake loading, respectively, are withstood by the lateral reaction of the soil against the monopile. Static moment due to wind and waves translates into additional horizontal stress applied to the soil adjacent to the leeward side of the monopile. In this region, negative pore pressure in the order of 15-20 kPa was recorded at a lateral distance of 1D from the monopile, meaning that soil tends to dilate (Fig. 13). However, the volume of dilative soil is small compared to the volume of soil beyond the dilative zone that undergoes liquefaction. Hence, the soil does not provide enough reaction force to counteract the stress applied by the monopile, resulting in substantial rotation of the OWT (Español-Espinel et al., 2024).

After the earthquake, pore water tends to migrate from the areas in which the excess pore water pressure is positive, to the dilative region adjacent to the monopile, leading to an increase in excess pore pressure in this region of the model. The soil, therefore, loses strength while the lateral static load remains applied to the structure. As a result, the offshore wind turbine (OWT) exhibits additional rotation until the excess pore pressure dissipates and the effective stress is sufficiently recovered.

Accepted manuscript doi:
10.1680/jgeot.24.01059

In the case of the monopile and outrigger combined, both the skin friction of the monopile and the base resistance of the skirted footings come into play to withstand the self-weight of the turbine. Therefore, this foundation experiences less settlement than the monopile or the outrigger alone. The excess pore pressure at 1D from the leeward side of the monopile appears to reach positive values similar to those observed in the far-field. Thus, the monopile is no longer transferring the stress resulting from lateral loading onto the soil (Fig. 13). Strong dilation is observed below the leeward skirted footing instead, meaning that the composite foundation relies on the skirted footings of the outrigger to resist the dynamic and static moments mainly.

The results summarised in Tables 6 and 7 suggest that the outrigger supported OWT experienced significantly less rotation, but larger settlements than the other foundation types. This is due to the mechanism through which the outrigger transfers the loads affecting the OWT onto the soil. First, the self-weight of the OWT is entirely withstood by the base resistance of the skirted footings. Hence, the outrigger transfers both the stress generated by the static and dynamic moments and the stress caused by the self-weight of the OWT directly onto the soil. In other words, the amount of vertical stress applied by the outrigger onto the soil is significantly higher than that transferred by the composite foundation.

As observed in Fig.14, suction below the outrigger is in general, much higher than that measured below the skirted footings of the composite foundation. Thus, the soil below the skirted footings of the outrigger relies on additional strength compared to the composite foundation while the lateral static loading and the dynamic loading act on the structure simultaneously. The legs of the outrigger provide additional lever arm and therefore, increased rotational stiffness, which

counteracts the moments generated by static and dynamic loads. Although the hybrid foundation took advantage from the lever arm provided by the legs as well, the stress applied onto the soil, and therefore, the additional strength due to suction was not as high. Therefore, the composite foundation experienced larger rotation compared to the outrigger during the earthquake.

The suction pressure bulbs generated below the individual skirted footings are not large enough to prevent settlement of the foundation into the liquefied ground below. Following the end of the earthquake, the pore water migrates from those regions where the excess pore pressure is positive, to the soil below the skirted footings of the outrigger, and the excess pore pressure tends to equalise with that recorded in the far-field (Fig. 14). Once the earthquake loading has ceased, the outrigger withstands only the self-weight of the OWT and the static lateral load. These loads drive additional settlement and rotation, although these are relatively small compared to the co-seismic values (see Tables 6 and 7).

The comparable or even superior performance of the outrigger system when subjected to seismic loading relative to that of the monopile and outrigger composite system represents a practical advantage. At first glance, skirted footings enable faster installation compared to monopiles. Therefore, adopting of the outrigger system could potentially reduce the installation costs of OWT foundations considerably.

CONCLUSIONS

In this paper, the main focus is on investigating alternative foundations systems for OWTs that offer better performance under seismic loading, particularly when liquefaction of shallow layers of sand is expected. Three types of foundations were investigated with the primary aim of

increasing rotational stability of the OWT under the combined action of operational environmental load and seismic load as recommended by DNV-RP-0585 (2021).

The findings of this research suggest that commonly adopted monopile foundations may not be the most effective solution to support OWTs in seismic areas at risk of liquefaction. This research proposes a new foundation type to support OWT in liquefiable soils based on the principle that full liquefaction of foundation soil may be avoided if large enough stress is transferred onto the soil. The proposed foundation is an outrigger that includes four legs with skirted footings at their ends.

The rotational stiffness of the three types of foundations was evaluated before, during and after a seismic event. It was shown that the proposed outrigger foundation with skirted footings offered the largest rotational stiffness both in pre and post seismic event scenarios. It was surprising that the composite foundation with monopile and skirted footings has lower rotational stiffness compared to the outrigger as a standalone foundation. This was attributed to the lower vertical effective stresses below the skirted footings in the composite case (as much of the vertical load is expected to be carried by the monopile), leading to a lower stiffness and hence larger overall rotations. During the seismic event itself, the evolution of pore pressures in the soil adjacent to the monopile and skirted footings is very different in each of the three cases considered.

Overall, the outrigger fully relies on the skirted footings to transfer the vertical load and moments to which the OWT is subjected in the form of vertical stress applied onto the soil. The outrigger design exhibits reduced rotation compared to the monopile and the composite system, although at the cost of higher settlements. However, the installation of a four skirted footings

foundation is simpler than installing a monopile, *i.e.*, requiring smaller jack-up rigs *etc.*, which could be advantageous for the industry.

ACKNOWLEDGEMENTS

The centrifuge experiments were performed with the excellent help of technicians at the Schofield Centre of University of Cambridge. This support is gratefully acknowledged.

The second author is grateful for the financial support provided by Ministero dell'Università e della Ricerca (Italy) through the project PON "Ricerca e Innovazione" 2014-2020.

Notations

D	monopile/skirted footings diameter
D_R	relative density
e	eccentricity = RNA height
e/D	eccentricity ratio
f_n	natural frequency
g	gravitational acceleration (= 9.81 m/s^2)
K□□	(secant) rotational stiffness of the soil-foundation systems
L	embedded length
L/D	aspect ratio
M	static moment at g.l.
PGA	*Peak Ground Acceleration*
u_{excess}	excess pore water pressure
u_{hyd}	hydrostatic pore water pressure
□$_{v0}$	geostatic total vertical stress
□'$_{v0}$	geostatic effective vertical stress

Accepted manuscript doi:
10.1680/jgeot.24.01059

References

Alkhoury, P., Soubra, A.H., Rey, V. & Aït-Ahmed M. (2020). Natural frequencies estimation of a monopile supported DTU-10 MW Offshore Wind Turbine. 4th International Symposium on Frontiers in Offshore Geotechnics ISFOG - Austin, Texas.

Anastasopoulos, I., Theofilou, M. (2016). Hybrid foundation for offshore wind turbines: Environmental and seismic loading. Soil Dynamics and Earthquake Engineering, 80, 126-209. ISSN 0267-7261.

Asareh, M.A., Schonberg, W., Volz, J., (2016). Effects of seismic and aerodynamic load interaction on structural dynamic response of multi-megawatt utility scale horizontal axis wind turbines. Renew. Energy;86:49–58. https://doi.org/10.1016/j.renene.2015.07.098.

Chen, W., Jiang, Y., Xu, L., Liu, C., Chen, G., Wang, P. (2023). Seismic response of hybrid pile-bucket foundation supported offshore wind turbines located in liquefiable soils. Ocean Engineering. 269, 113519. ISSN 0029-8018.

Brennan, A. J., Madabhushi, S. P. G. & Houghton, N. E. (2006). Comparing laminar and equivalent shear beam (ESB) containers for dynamic centrifuge modelling. Proc. 6th Int. Conf. Phys. Mod. Geotech., ICPMG 2006. Leiden: Taylor and Francis, 171-176.

Esfeh, P. K., & Kaynia, A. M. (2020). Earthquake response of monopiles and caissons for Offshore Wind Turbines founded in liquefiable soil. Soil Dynamics and Earthquake Engineering, 136, 106213. DOI: https://doi.org/10.1016/j.soildyn.2020.106213

Español-Espinel, C., Haigh, S. K., & Madabhushi, S. P. G. (2023). Liquefaction analysis of soil plugs within large diameter monopiles using numerical modelling. Bulletin of Earthquake Engineering, 21, No. 12, 5443-5458. DOI: 10.1007/s10518-023-01742-7

Español-Espinel, C., Haigh, S. K., Madabhushi, S. P. G., Abadie, C. N., Go, J. E. & Morrison, P. R. J. (2024). Evolution of excess pore water pressures around monopiles subjected to moderate seismic loading. Soil Dynamics and Earthquake Engineering, 176, 108316. DOI: 10.1016/j.soildyn.2023.108316

DNV-ST-0126. (2021). Support structures for wind turbines. Standard DNV-ST-0126.

DNV-RP-0585. (2021). Seismic design of wind power plants recommended practice.

Gaudio, D., Seong, J., Haigh, S. K., Viggiani, G. M. B., Madabhushi, S. P. G., Shrivatsava, R., Veluvolu, R. & Padhy, P. (2023). Boundary effects on dynamic centrifuge modelling of onshore wind turbines on liquefiable soils, International Journal of Physical Modelling in Geotechnics,

ICE Publishing, 23, No. 1, 16-34, ISSN: 1346-213X. DOI: https://doi.org/10.1680/jphmg.21.00085

Haigh, S. K. & Madabhushi, S. P. G. (2005). The effects of pile flexibility on pile-loading in laterally spreading slopes. Workshop on Seismic Performance and Simulation of Pile Foundations in Liquefied and Laterally Spreading Ground. ASCE, Special Publication 145, 24-37. https://doi.org/10.1061/40822(184)3

Kaynia, A.M. (2018). Seismic considerations in design of offshore wind turbines. Soil Dynamics and Earthquake Engineering. https://doi.org/10.1016/j.soildyn.2018.04.038.

Kutter, B.L. & Wilson, D.W. (1999). De-liquefaction shock waves. Proceedings, 7th US-Japan workshop on earthquake resistant design of lifeline facilities and countermeasures against soil liquefaction, MCEER-99-0019: 295-310.

Madabhushi, S. P. G., Houghton, N. E. & Haigh, S. K. (2006). A new automatic sand pourer for model preparation at the University of Cambridge. Proc. 6th Int. Conf. Phys. Mod. Geotech., ICPMG 2006. Leiden: Taylor and Francis, 217-222.

Madabhushi, S. P. G. & Haigh, S. K. (2012). How well do we understand earthquake induced liquefaction? Indian Geotechnical Society Journal, 42, No. 3, 150-160. DOI: 10.1007/s40098-012-0018-2

Madabhushi, S. P. G. (2014). Centrifuge modelling for civil engineers. Boca Raton, FL, USA: CRC Press, Taylor & Francis Group

Madabhushi, S. P. G., Haigh, S. K., Houghton, N. E. & Gould, E. (2015). Development of a servo-hydraulic earthquake actuator for the Cambridge Turner beam centrifuge. International Journal of Physical Modelling in Geotechnics, 12, No. 2, 77-88, https://doi.org/10.1680/ijpmg.11.00013

Natarajan, K., & Madabhushi, S. P. G. (2022). Seismic response of an offshore wind turbine jacket structure with pile foundations. Soil Dynamics and Earthquake Engineering, 162, 107427.

Shadlou, M., & Bhattacharya, S. (2016). Dynamic stiffness of monopiles supporting offshore wind turbine generators. Soil Dynamics and Earthquake Engineering, 88, 15-32.

Shakeran, M., Soroush, A. (2024). Centrifuge testing on ordinary and hybrid suction caissons subjected to cyclic lateral loading. Ocean Engineering, 300, 117471.

Shaofeng, W., Torben Juul, L., and Bredmose, H. (2021). Ultimate load analysis of a 10 MW offshore monopile wind turbine incorporating fully nonlinear irregular wave kinematics. Marine Structures, 76:102922.

Smith, V., Mahmoud, H. (2016) Multihazard assessment of wind turbine towers under simultaneous application of wind, operation, and seismic loads. Journal Perform Constr. Facil ASCE; 4016043(6):30. https://doi.org/10.1061/(ASCE)CF. 1943-5509.0000898.

Stringer, M. E. & Madabhushi, S. P. G. (2009). Novel computer-controlled saturation of dynamic centrifuge models using high viscosity fluids. Geotechnical Testing Journal, 32, No. 6, 559-564.

Stringer, M. E. & Madabhushi, S. P. G. (2011). The effect of pile installation method on dynamic pile response. International Journal of Physical Modelling in Geotechnics. 11 (3), 87-99.

Accepted manuscript doi:
10.1680/jgeot.24.01059

Tables

Table 1. Comparison of properties between the prototype monopile-supported offshore wind turbine (OWT) and the DTU 10 MW reference offshore wind turbine (Shaofeng *et al*., 2021).

Properties	Symbol	Prototype Structure	Real Structure
Diameter [m]	*D*	4	9
Embedded Length [m]	*L*	17.5	42.6
RNA height [m]	*e*	53.30	149
Aspect Ratio	*L/D*	4.38	4.73
Eccentricity Ratio	*e/D*	13.33	16.56
Static Loading at the RNA [MN]	*H*	0.367	1.5
Static Moment at G.L. [MNm]	*M*	20	278

Table 2. Properties of the skirted footings of the outrigger foundation at prototype scale

Properties	Symbol	Prototype Structure
Diameter [m]	*D*	3.15
Embedded Length [m]	*L*	3.50
Aspect Ratio	*L/D*	1.11

Table 3. Factor of safety to vertical load for the monopile, the monopile and outrigger, and the outrigger as a standalone structure.

Foundation Type	Mass of OWT and Foundation [Mg]	Vertical Load [MN]	Vertical Capacity [MN]	Factor of Safety
Monopile	2095.62	20.56	59.83	2.91
Monopile and Outrigger	2784.85	27.32	137.88	5.05
Outrigger	2627.39	25.77	78.05	3.03

Accepted manuscript doi:
10.1680/jgeot.24.01059

Table 4. Loading sequence of the experiment. This paper focuses on the results extracted from earthquakes EQ1 and EQ2 for brevity.

Earthquake	**Peak Ground Acceleration [g]**	**Frequency [Hz]**	**Cycles**	**Static Moment at g.l. [MNm]**
EQ1	0.03	0 - 5	Sine sweep	0
				Loading
EQ2	0.18	1 Hz	10	20
				Unloading
EQ3	0.23	1 Hz	10	0
				Reloading
EQ4	0.26	1 Hz	10	20

Table 5. Secant rotational stiffness of the three foundation systems (units: GN·m/rad)

Foundation	Loading	Unloading	Reloading
Monopile	4.63	4.66	5.17
Monopile and outrigger	7.05	6.21	6.00
Outrigger	9.66	9.85	32.31

Table 6. Accumulated rotation of the OWT for the three foundation systems.

Foundation	Co-seismic		Post-seismic		Total
	degrees	%	degrees	%	degrees
Monopile	2.50	87.7	0.35	12.3	2.85
Monopile and outrigger	0.60	92.3	0.05	7.7	0.65
Outrigger	0.30	60.0	0.20	40.0	0.50

Table 7. Accumulated average settlement experienced by the OWT for the three foundation systems.

Foundation	Co-seismic		Post-seismic		Total
	mm	%	mm	%	mm
Monopile	285	89.3	34	10.7	319
Monopile and outrigger	130	92.9	10	7.1	140
Outrigger	365	79.0	97	21.0	462

Accepted manuscript doi:
10.1680/jgeot.24.01059

Figure captions

Fig. 1. Typical dimensions and loads carried by a DTU 10 MW reference offshore wind turbine supported by a monopile foundation (modified after Shaofeng *et al*., 2021).

Fig. 2. Monopile supported offshore wind turbine at prototype scale.

Fig. 3. Centrifuge models at prototype scale: (a) monopile and outrigger composite foundation, and (b) outrigger only.

Fig. 4. Side view (top) and top view (bottom) of the outrigger.

Fig. 5. Moment-rotation response of the three foundations systems under static loading. Monopile (left), Outrigger and monopile (middle) and outrigger only (right).

Fig. 6. Fast Fourier Transform of the prototype OWT supported by the monopile, the monopile and outrigger, and the outrigger. The first and second excitation modes of a DTU 10 MW OWT, as calculated by Alkhoury *et al*., 2020, are superimposed. The input acceleration of EQ1 is depicted at the bottom.

Fig.7 Moment at ground level obtained from the load cell when the monopile supported OWT is subjected to a combination of static lateral loading and dynamic loading from EQ2 (blue). Dynamic moment at ground level calculated using the acceleration of the RNA in the laterally loaded scenario (red). Dynamic moment at ground level calculated using the acceleration of the RNA in the non-laterally loaded scenario (green).

Fig. 8. Excess pore water pressure recorded across the vertical array of sensors located in the far-field.

Fig. 9. Time histories of moment at ground level (top) and rotation (middle) experienced by the foundation systems considered in the study. The input motion is shown at the bottom.

Fig. 10. Moment-rotation response of the monopile foundation, during and after applying the input motion.

Fig. 11. Moment-rotation response of the three foundations systems considered in the study, during and after applying the input motion.

Fig. 12. Time histories of moment at ground level (top) and average settlement (middle) experienced by the foundation systems considered in the study. The input motion is displayed at the bottom.

Fig. 13. Co-seismic and post-seismic induced rotation (top) experienced by the monopile and the composite system. Excess pore water pressure recorded at 1 monopile diameter from the leeward side of the monopile (PPT-259) and from the monopile of the composite foundation (PPT-240), at a depth of z = 2.94 m (middle). The input motion is displayed at the bottom.

Fig. 14. Co-seismic and post-seismic induced rotation (top) experienced by the monopile and outrigger composite system and the outrigger only. Excess pore water pressure recorded below the leeward skirted footing of the composite foundation (PPT-251) and beneath the leeward skirted footing of the outrigger (PPT-250) at a depth of z = 4.76 m (middle). The input motion is displayed at the bottom.

Fig. 15. Excess pore water pressure recorded below the windward (PPT-260) and leeward (PPT-232) skirted footings of the outrigger, as well as at the far-field (PPT-224), at a depth of z = 5.95 m. The input motion of EQ2 is displayed at the bottom.

Accepted manuscript doi:
10.1680/jgeot.24.01059

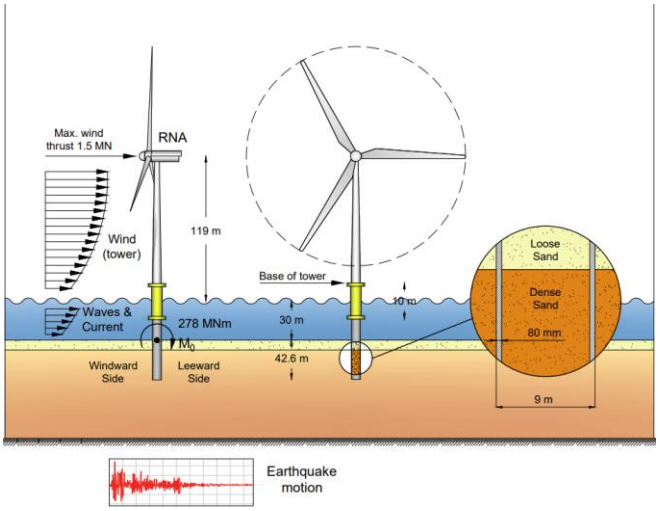

Fig. 1

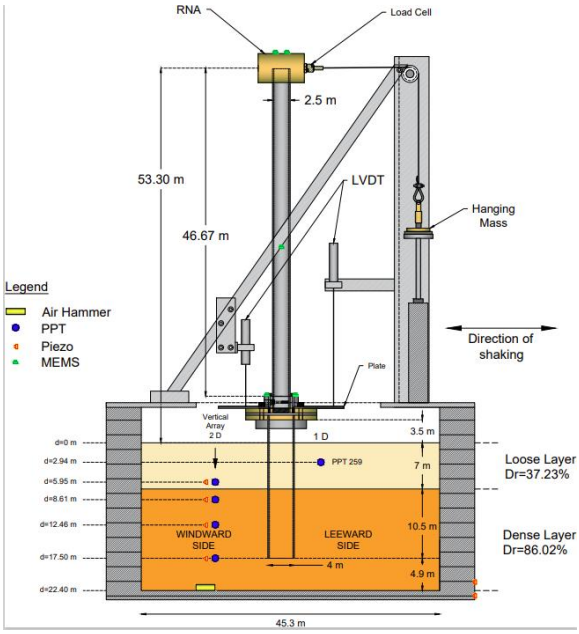

Fig. 2

Accepted manuscript doi:
10.1680/jgeot.24.01059

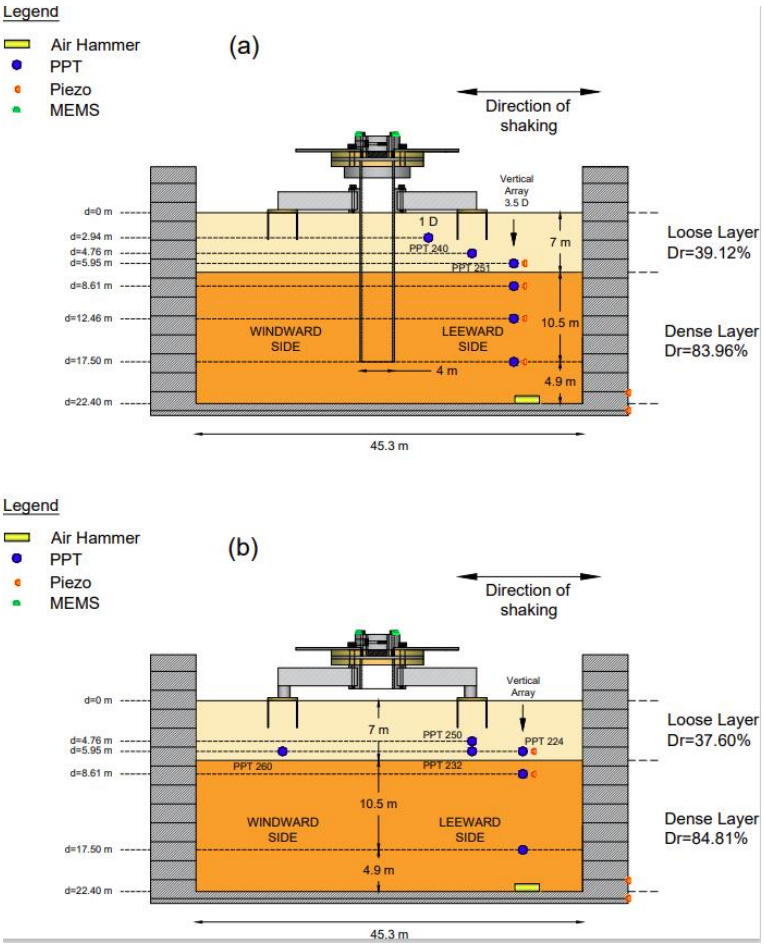

Fig. 3

Accepted manuscript doi:
10.1680/jgeot.24.01059

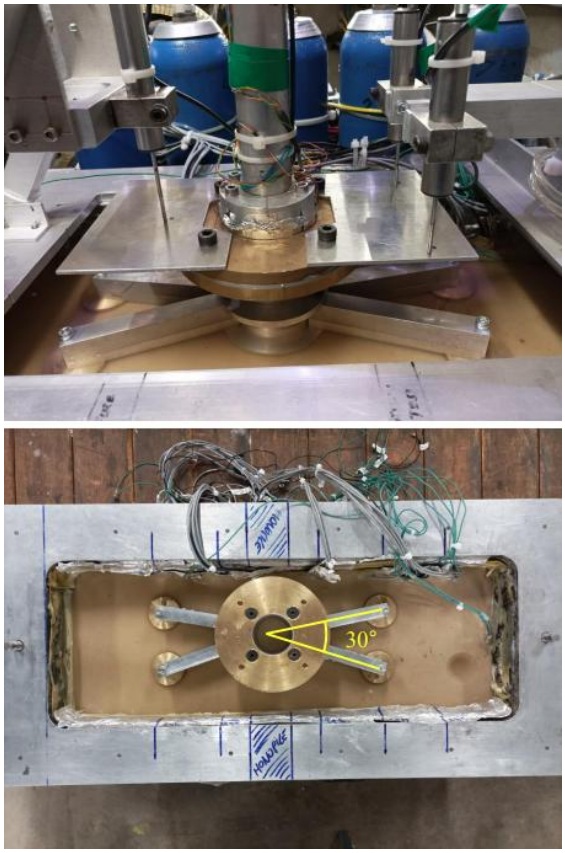

Fig. 4

Accepted manuscript doi:
10.1680/jgeot.24.01059

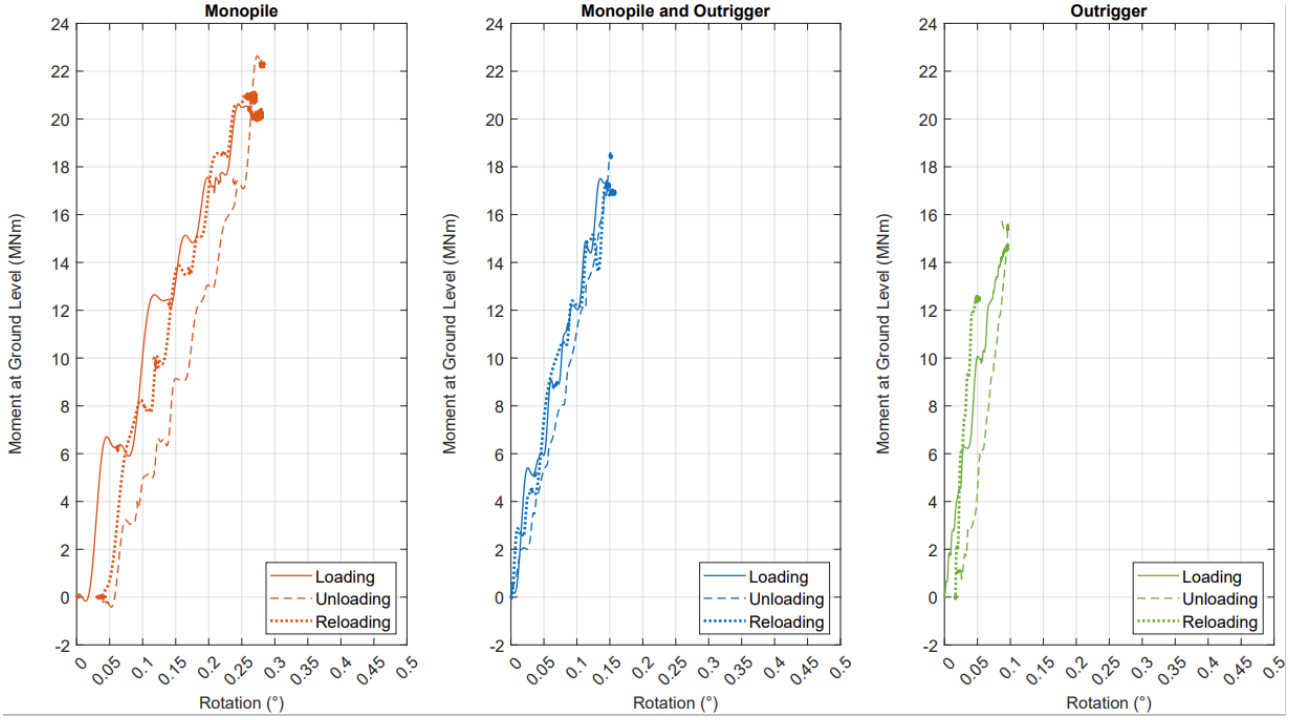

Fig. 5

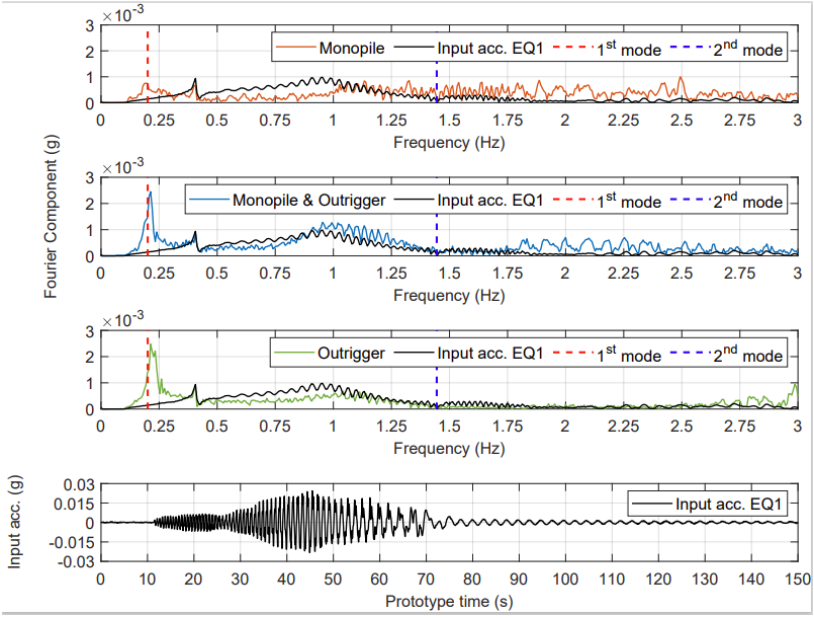

Fig. 6

Accepted manuscript doi:
10.1680/jgeot.24.01059

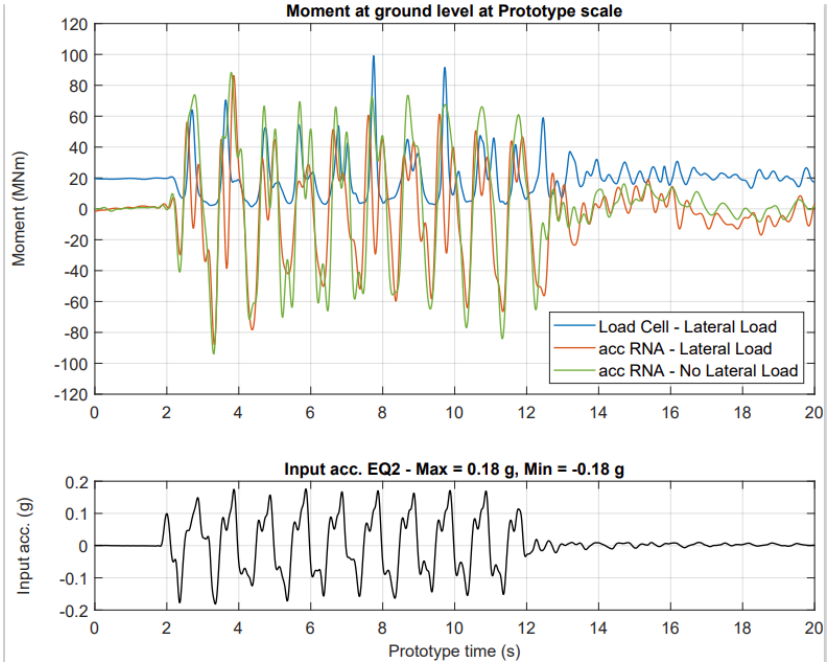

Fig. 7

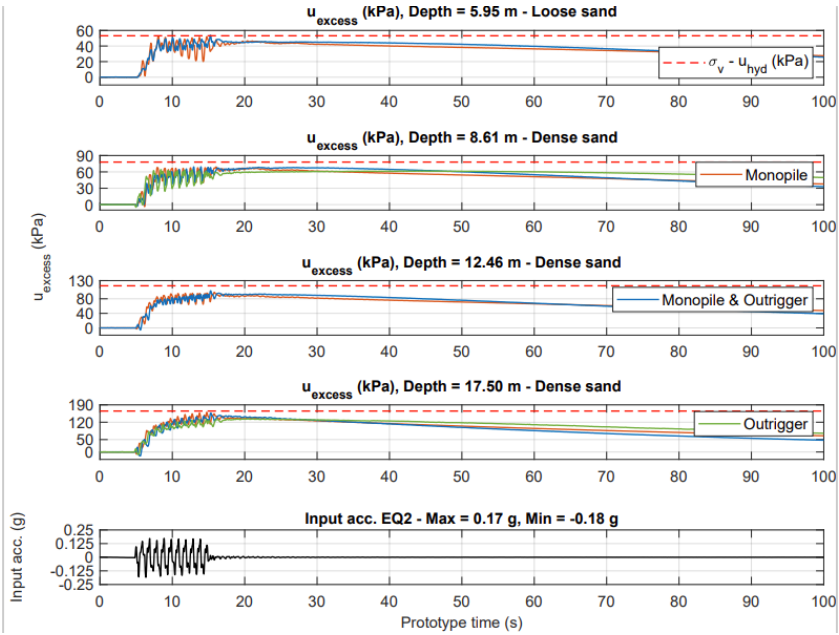

Fig. 8

Accepted manuscript doi:
10.1680/jgeot.24.01059

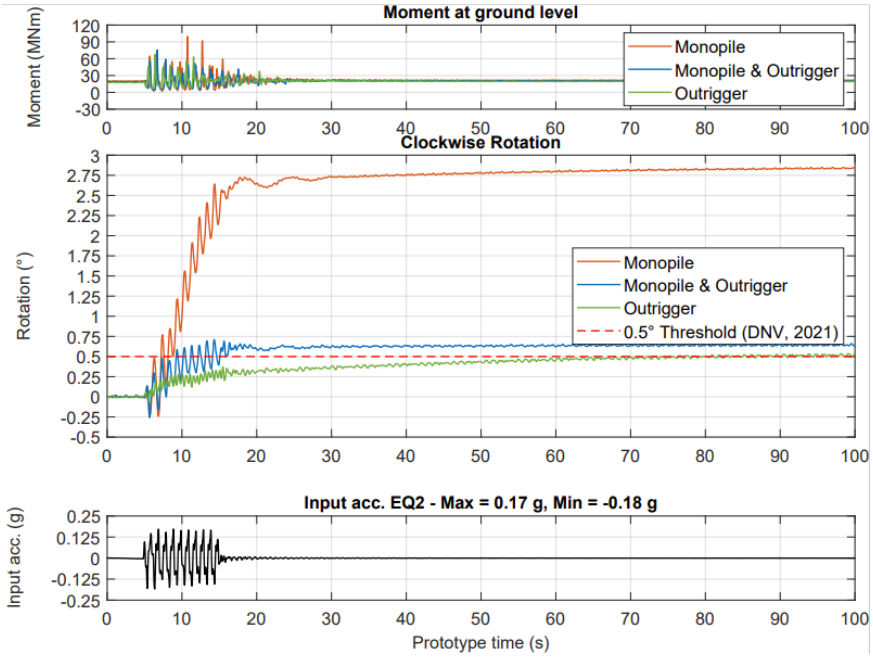

Fig. 9

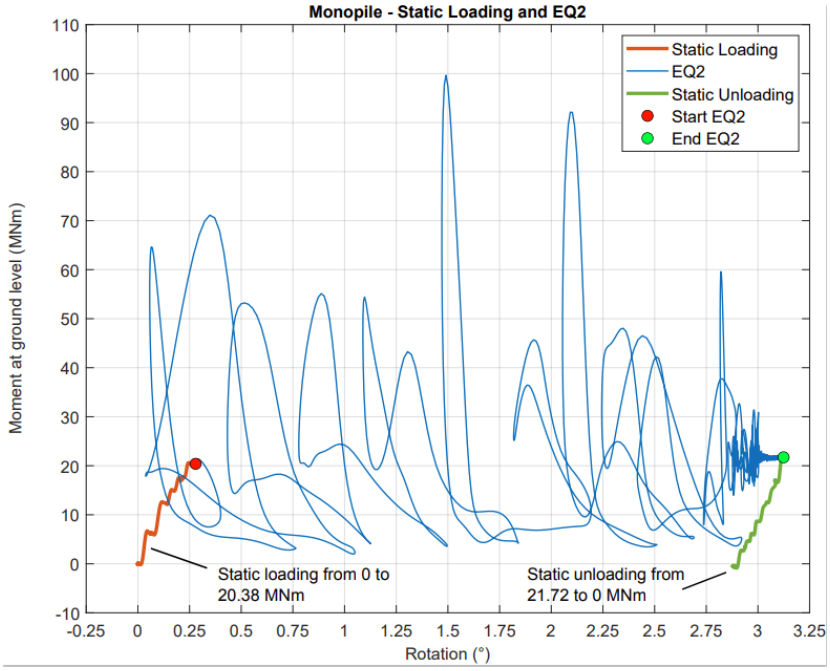

Fig. 10

Accepted manuscript doi:
10.1680/jgeot.24.01059

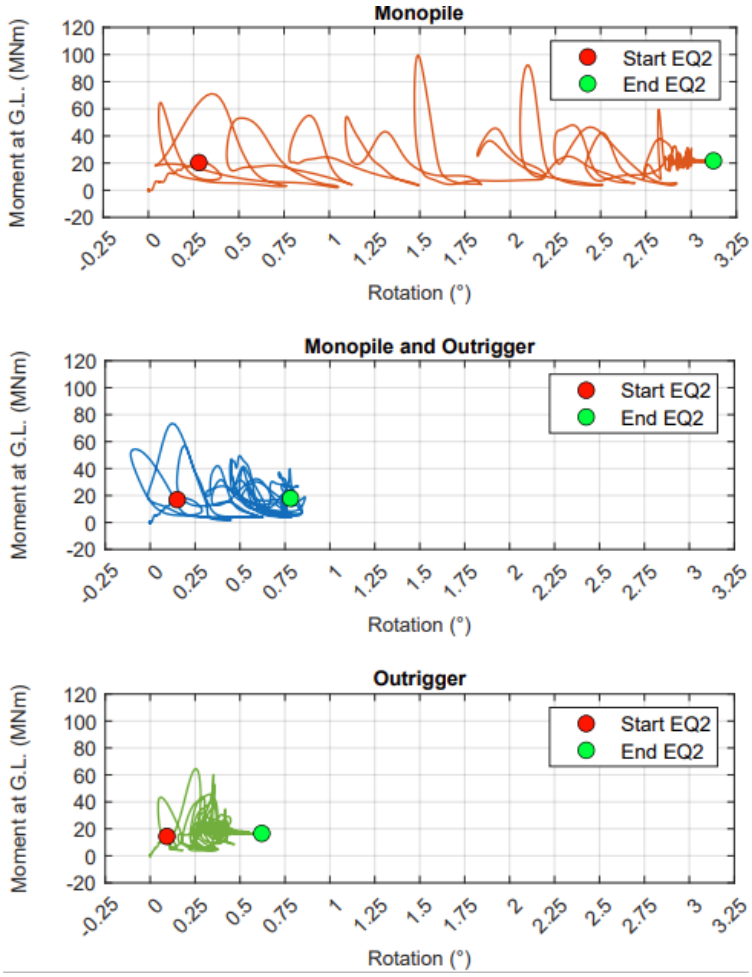

Fig. 11

Accepted manuscript doi:
10.1680/jgeot.24.01059

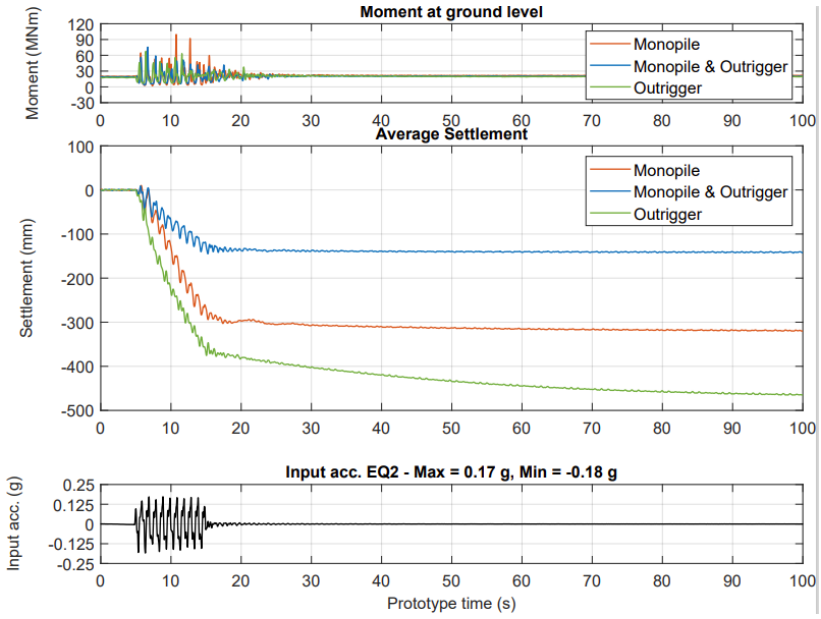

Fig. 12

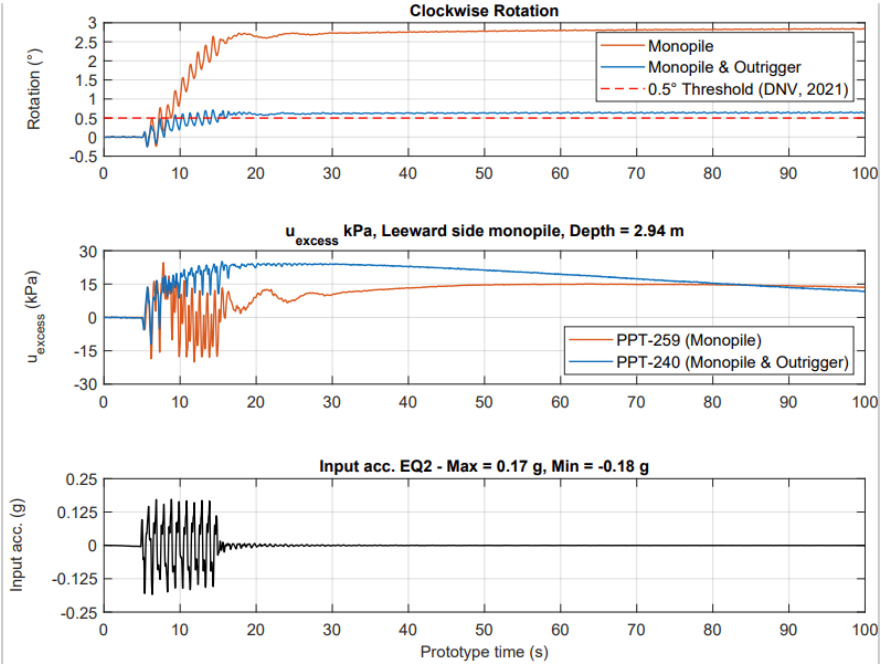

Fig. 13

Accepted manuscript doi:
10.1680/jgeot.24.01059

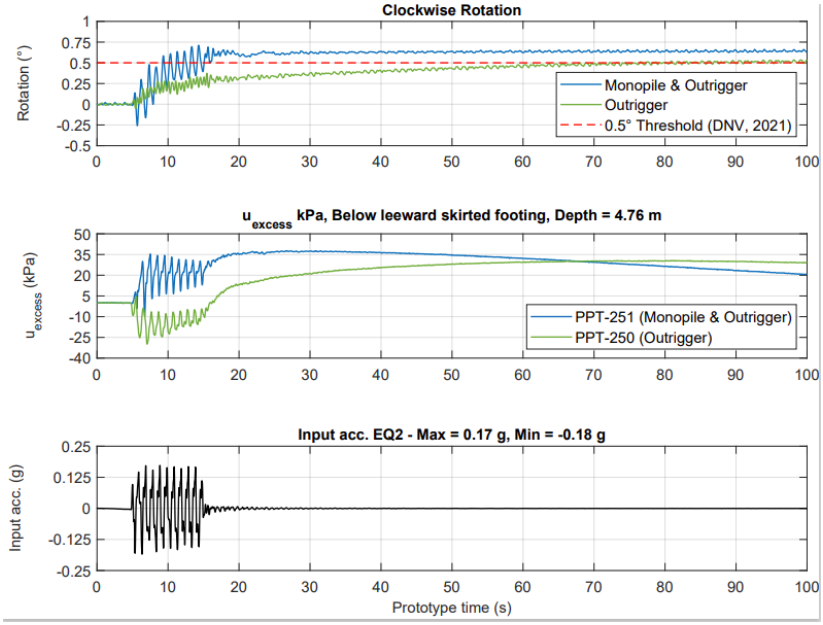

Fig. 14

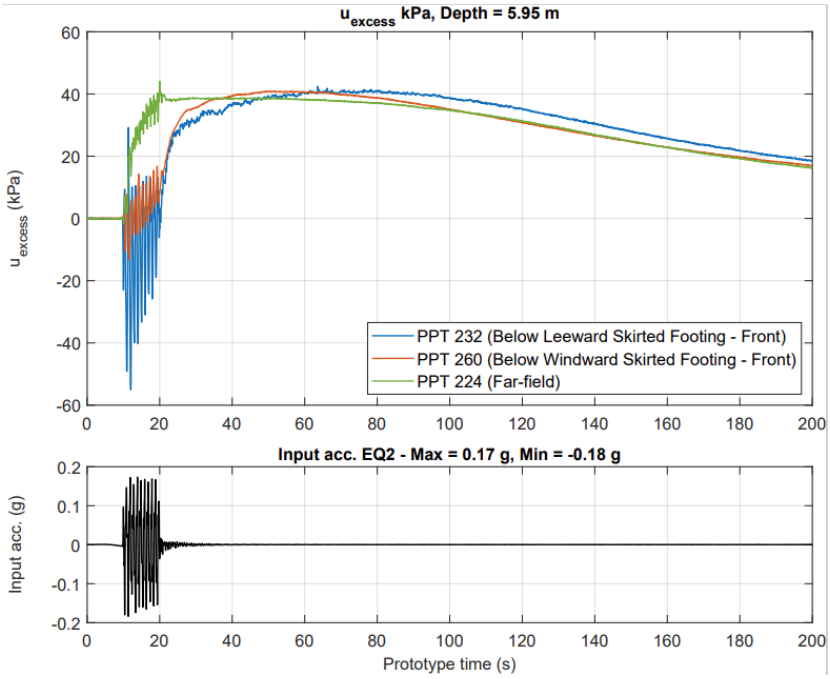

Fig. 15